Twist Propagation in Dinucleosome Arrays

Irina V. Dobrovolskaia,[△] Martin Kenward,[△] and Gaurav Arya*
Department of NanoEngineering, University of California at San Diego, La Jolla, California

ABSTRACT We present a Monte Carlo simulation study of the distribution and propagation of twist from one DNA linker to another for a two-nucleosome array subjected to externally applied twist. A mesoscopic model of the array that incorporates nucleosome geometry along with the bending and twisting mechanics of the linkers is employed and external twist is applied in stepwise increments to mimic quasistatic twisting of chromatin fibers. Simulation results reveal that the magnitude and sign of the imposed and induced twist on contiguous linkers depend strongly on their relative orientation. Remarkably, the relative direction of the induced and applied twist can become inverted for a subset of linker orientations—a phenomenon we refer to as "twist inversion". We characterize the twist inversion, as a function of relative linker orientation, in a phase diagram and explain its key features using a simple model based on the geometry of the nucleosome/linker complex. In addition to twist inversion, our simulations reveal "nucleosome flipping", whereby nucleosomes may undergo sudden flipping in response to applied twist, causing a rapid bending of the linker and a significant change in the overall twist and writhe of the array. Our findings shed light on the underlying mechanisms by which torsional stresses impact chromatin organization.

INTRODUCTION

During transcription and replication, the unzipping of double-stranded DNA can produce strong torsional forces (1,2). For instance, an advancing RNA polymerase can exert torques as large as ~1.25 k_BT/rad (where k_BT is the thermal energy) (3), resulting in over- and undertwisted DNA ahead and behind it, respectively (4). Such torsional forces may locally distort the DNA structure (5), and, if sufficiently severe, induce conformational changes, such as that from B- to A- and Z-DNA (6). Concurrently, applied torsion could have global effects leading to the formation of DNA loops, solenoids, and plectonemes (7).

The local and global torsional response of DNA can strongly impact its biological activity. Structural distortions of DNA can alter its binding affinity for proteins such as transcription factors, thus influencing gene transcription (8). Twist-dependent protein/DNA binding has also been suggested as an indirect-readout mechanism for protein/DNA recognition (9,10). DNA supercoiling can alter the accessibility of DNA to protein binding (8,9,11) and the juxtaposition probabilities of distant DNA sites, potentially affecting genetic recombination. Given its importance, it is not surprising that DNA supercoiling is tightly regulated inside cells. In fact, an entire class of enzymes, the topoisomerases, are devoted to removing excess positive and negative supercoils from DNA (12,13). Emerging evidence also suggests that supercoiling is not an entirely unfavorable byproduct of transcription; it may instead serve to signal protein binding over long genomic distances (2,14).

Significant progress has been made in understanding the torsional behavior of naked DNA. The topology of circular or closed DNA is described by two variables: the twist Tw and the writhe Wr. The linking number Lk provides a relationship between Tw and Wr. For closed or end-constrained DNA, Lk is topologically invariant and equal to the sum of the twist and the writhe, $Lk = Tw + Wr$ (15). A key issue in the field has been understanding how torsionally stressed DNA, characterized by the deviation of Lk from its relaxed value Lk_0, distributes its stresses internally through changes in twist and writhe. Torsional stresses in open DNA can result from external twisting of its ends and in circular DNA through internal cutting, crossing, and rejoining of single strands by topoisomerases (12,13,16). Extensive studies have examined the relationship between Tw and Wr during the relaxation of torsionally-stressed DNA including the effects of torsional and bending rigidity and the presence of binding proteins (10). A large body of work has also elucidated various forms of local structural changes associated with twisted DNA, by using both experimental (17,18) and theoretical approaches (15,19–21).

The majority of studies have primarily focused on the torsional properties of naked (prokaryotic) DNA. Therefore, most studies are not relevant to eukaryotic DNA, which is rarely present in its naked form. Eukaryotic DNA is instead wrapped around histone octamers to form nucleosomes (22). Naked DNA is only present in short intervening sections between nucleosomes, typically 20–70 basepairs (bp) in length, and referred to as linker DNAs or linkers. Under physiological conditions, the chain of nucleosomes folds into a compact, 30-nm thick chromatin fiber, which in turn compacts into higher-order structures (23).

We ask, how are the torsional properties of DNA affected by its organization into chromatin?

Submitted July 13, 2010, and accepted for publication September 28, 2010.

[△]Irina Dobrovolskaia and Martin Kenward contributed equally to this work.

*Correspondence: garya@ucsd.edu

Editor: Ruth Nussinov.

0006-3495/10/11/3355/10 $2.00

doi: 10.1016/j.bpj.2010.09.055

First, the strong electrostatic binding of DNA to the histone octamer is expected to critically hinder the propagation of torsional stresses between consecutive linkers along the wound DNA (2). Second, as a result of hindered twist propagation, chromatin may instead relax its torsional stress through rigid-body-like nucleosome rotations or nucleosome flipping. The latter has been predicted to occur in the single-chromatin fiber twisting experiments of Bancaud et al. (3,24). Third, the DNA within chromatin is subjected to significant steric constraints from nucleosomes and internucleosomal interactions mediated by histone tails. Moreover, the strong twist/bend coupling in DNA may be exacerbated in chromatin due to such steric constraints, thus modulating chromatin torsional stresses in an as-yet-unknown manner.

To date, few studies have examined the torsional behavior of chromatin (3,24,25). Bancaud et al. (3,24) used magnetic tweezers to twist individual reconstituted nucleosome arrays at fixed stretching forces. The arrays were found to accommodate large torsional stresses without significant changes in its length, in sharp contrast to DNA. Moreover, the length variations were found to be highly asymmetric with respect to applied twist direction. The authors proposed a model for these variations based on nucleosome flipping, which modulated the entry/exit linker conformation (3,24). Recent single-molecule twisting studies (26) have confirmed chromatin's lower torsional rigidity compared to naked DNA. Other studies have examined the functional consequences of transcription-generated DNA supercoiling in eukaryotic organisms. For example, Kouzine et al. (14) have shown that torsional stresses can propagate over kbp domains in chromatin, promoting formation of non-B-DNA structures that signal binding of specific proteins. The above studies represent only the tip-of-the-iceberg, and undoubtedly, many more investigations will provide additional quantitative results on the microscopic torsional mechanics of chromatin and its regulatory roles in biology.

In this study, we show that simple computational models can be used to obtain new insights into the torsional behavior of chromatin. Specifically, we examine the propagation of torsional stress from one linker to the next, across a single nucleosome. Our simulations yield two intriguing findings. First, the magnitude and sign of applied-versus-induced twist in the linkers is dictated by their relative orientation. A subset of these orientations leads to opposite twist direction in consecutive linkers, a phenomenon we refer to as "twist inversion". We propose a simple physical explanation of twist inversion based on the geometry of the linker DNA/nucleosome complex. Second, we observe a phenomenon analogous to buckling in twisted semirigid rods, whereby the nucleosome undergo sudden flipping in response to continued applied twist. Nucleosome flipping can induce drastic changes in the conformation of the dinucleosome and its overall writhe. We discuss the potential relevance of our findings to chromatin's ability to absorb applied twist, higher-order folding of chromatin, and functional regulation of chromatin through mechanical stresses.

MODEL AND SIMULATION METHODS

Linker and nucleosome model

Our model system, shown schematically in Fig. 1, contains two nucleosomes and two DNA linkers, which we refer to as a dinucleosome array or a dinucleosome. One end (the nucleosome) is held fixed and the other end (the linker) is twisted to examine how twist propagates from one linker to the next across the central nucleosome. The dinucleosome thus represents the most fundamental unit of chromatin for examining its torsional properties. It allows us to extract the essential physics governing propagation of twist across the chromatin fiber that is not affected by other more complex effects such as internucleosomal interactions and torsional forces arising from fluctuations in neighboring nucleosomes.

We model the dinucleosome based on previous work (27,28), but simplify some aspects of it. The linker is composed of six contiguous charged beads to mimic the 60-bp linkers of chicken erythrocyte chromatin (27,28). Each linker bead (Fig. 1) represents a 3-nm-long section of double-stranded DNA. Linkers are ascribed interaction potentials that account for: salt-dependent electrostatics, stretching, bending, and twisting mechanics, and excluded volume interactions between other linker and nucleosomes.

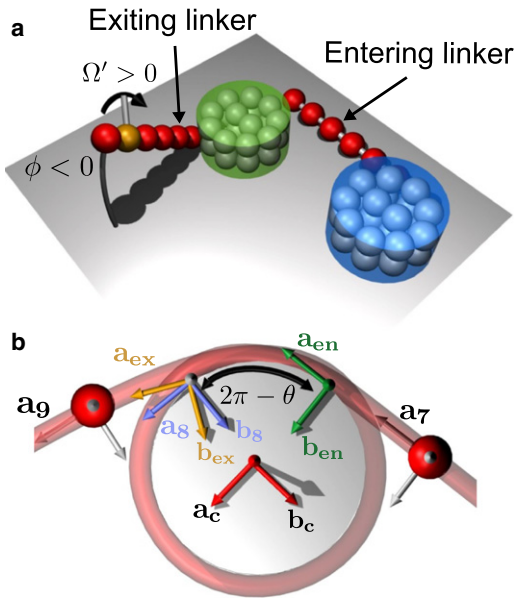

FIGURE 1 (*a*) Dinucleosome array showing the orientation of the two linkers (*red*), as defined by the entry/exit angle θ and azimuthal angle ϕ. The rightmost nucleosome (*blue*), penultimate (*orange*), and last linker beads are spatially and rotationally constrained in our twisting simulations. (*b*) Nucleosome and linker bead coordinate systems. See text for details.

The linker connected to the first nucleosome (*blue*) is termed "entering" and the end linker is termed "exiting". The nucleosome is composed of two stacks of beads, each of radius 1.5 nm. Each stack contains 11 beads: nine beads are evenly spaced in a ring of radius 4.3 nm and two are placed diametrically opposite to each other inside the ring (see Fig. 2). All beads are fixed in space to model a rigid nucleosome. This simplified model allows us to clearly delineate effects of nucleosome-linker geometry and linker torsion in modulating the conformation of the dinucleosome without interference from more complicated effects arising from linker histones and histone tails. Our choice for a simpler model of the nucleosome is also motivated by observations that more-detailed models exhibit essentially similar torsional behavior but are significantly more computationally demanding. Moreover, the simple dinucleosome system allows us to dissect twist propagation without the higher-order competing effects present in larger arrays (see the Supporting Material).

Dinucleosome mechanics and energetics

To account for bending and torsion in the system, local coordinate systems are ascribed to each nucleosome and linker bead. Nucleosome orientations are prescribed by a set of orthonormal unit vectors, $\mathbf{\Gamma}_c \equiv \{\mathbf{a}_c, \mathbf{b}_c, \mathbf{c}_c\}$, where $\mathbf{a}_c$ and $\mathbf{b}_c$ lie in the plane defined by the flat surface of the nucleosome. The values $\mathbf{a}_c$ and $\mathbf{b}_c$ point in directions tangential and normal (inwards) to the nucleosomal at the point of attachment of the exiting linker, respectively, and $\mathbf{c}_c = \mathbf{a}_c \times \mathbf{b}_c$ (Fig. 1).

The linker coordinate systems are denoted by $\mathbf{\Gamma}_i \equiv \{\mathbf{a}_i, \mathbf{b}_i, \mathbf{c}_i\}$, where i is the linker bead index and $\mathbf{a}_i$ points from bead i to $i + 1$. Two additional coordinate systems are defined. The coordinate system of the exiting linker attachment is denoted by $\mathbf{\Gamma}_{ex} \equiv \{\mathbf{a}_{ex}, \mathbf{b}_{ex}, \mathbf{c}_{ex}\}$. The two coordinate systems $\mathbf{\Gamma}_c$ and $\mathbf{\Gamma}_{ex}$ are identical. The coordinate system of the entering linker attachment is denoted by $\mathbf{\Gamma}_{en} \equiv \{\mathbf{a}_{en}, \mathbf{b}_{en}, \mathbf{c}_{en}\}$, where $\mathbf{a}_{en}$ and $\mathbf{b}_{en}$ are tangential and normal to the attachment, respectively, and $\mathbf{c}_{en}$ is defined by $\mathbf{c}_{en} = \mathbf{a}_{en} \times \mathbf{b}_{en}$.

Sets of Euler angles provide the transformation between consecutive coordinate systems. Euler angles $\{\alpha_i^+, \beta_i^+, \gamma_i^+\}$ provide transformations from the nucleosome coordinate system to the exiting site coordinate system on the nucleosome. To ensure that the nucleosome-wound DNA with zero twist does not impart any twist to the exiting linker, $\alpha_i^+ + \gamma_i^+$ is set to zero (28). Transformations between all other coordinate systems are given by $\{\alpha_i, \beta_i, \gamma_i\}$, where i denotes the index of the linker bead, or the nucleosome, or the entering linker sites. More-detailed descriptions of coordinate systems and Euler angles are available elsewhere (27 ,28).

The total energy of the dinucleosome (E_T) is given by the sum of five contributions from stretching (E_{str}), bending (E_{bend}), torsion (E_{Tw}), electrostatic (E_C), and excluded volume energies (E_{EV}), i.e.,

$$E_T = E_{str} + E_{bend} + E_{Tw} + E_C + E_{EV}. \quad (1)$$

The stretching energy of linker segments is given by

$$E_{str} = \frac{\kappa_{str}}{2}\sum_{i=1}^{N-1}(l_i - l_0)^2, \quad (2)$$

where κ_{str}, l_i, and l_0 are the stretching constant, linker segment length, and equilibrium segment length, respectively. The summation in Eq. 2 is carried out over the $N = 14$ nucleosomes and linker beads. The bending energy is given by

$$E_{bend} = \frac{\kappa_{bend}}{2}\left[\left(\beta_1^+\right)^2 + \left(\beta_2^+\right)^2 + \sum_{i=1}^{N-2}\beta_i^2\right], \quad (3)$$

where κ_{bend} and β_i are the bending energy constant and the Euler angle describing the local bending of the linker, respectively. The torsional energy is given by

$$E_{Tw} = \frac{\kappa_{Tw}}{2l_0}\sum_{i=1}^{N-2}(\alpha_i + \gamma_i)^2, \quad (4)$$

where κ_{Tw} and $\alpha_i + \gamma_i$ are the torsional energy constant and the Euler angles describing the twist between consecutive local coordinate systems, respectively.

The total linker-linker, linker-nucleosome, and internucleosome electrostatic energy, treated using the Debye-Hückel potential, is given by

$$E_C = \sum_{i=1}^{N_{bead}-1}\sum_{j=i+2}^{N_{bead}}\frac{q_i q_j}{4\pi\epsilon_0\epsilon r_{ij}}\exp\left(-\kappa_{DH} r_{ij}\right), \quad (5)$$

where q_i and q_j are the charges on beads i and j and r_{ij} is the center-to-center distance between the beads. N_{bead} is the total number of linker and nucleosome beads. The other parameters in Eq. 5 are ϵ, the dielectric constant of the medium; κ_{DH}, the inverse Debye screening length (27,28); and ϵ_0, the permittivity of free space.

Finally, the total linker-nucleosome, linker-linker, and internucleosome Lennard-Jones excluded volume interactions are given by

$$E_{EV} = \kappa_{ev}\sum_{i=1}^{N_{bead}-1}\sum_{j=i+2}^{N_{bead}}\left[\left(\frac{\sigma}{r_{ij}}\right)^{12} - \left(\frac{\sigma}{r_{ij}}\right)^{6}\right], \quad (6)$$

where κ_{ev} is an energy parameter and σ is the effective diameter of the beads constituting the linker and nucleosomes.

The summations in Eqs. 5 and 6 are over all beads for simplicity of notation. However, no excluded volume or electrostatic interactions between intranucleosome beads and contiguous linker beads exist. Relevant parameters are provided in the Supporting Material.

Monte Carlo twisting protocol

We implement quasistatic twisting of the dinucleosome array using a Monte Carlo (MC) approach. The initial linker and nucleosome positions are similar to that in Fig. 1, for a particular θ and ϕ. The entry/exit angle θ is defined as the angle between the two linker attachment points on the nucleosome and ϕ is the angle made by the exiting linker with the plane of the two nucleosomes. The rightmost nucleosome (*blue*) in Fig. 1 *a* is torsionally and translationally constrained; the other (*green*) nucleosome is free to move and rotate. The penultimate and last linker beads labeled 13 and 14, respectively, in Fig. 2 are also fixed in space.

Before twist application, the dinucleosome is first allowed to equilibrate (relax), subject to the constraints mentioned above. All equilibration phases are carried out using the Metropolis MC method at constant temperature. Two MC moves are used (27): The first is rotation of a randomly chosen bead or nucleosome by a random angle in interval $[-\delta_r, \delta_r]$ ($\delta_r = 0.3$ rad). While linker bead rotations are only implemented about its $\mathbf{a}_i$ axis, nucleosome rotations are chosen randomly about its $\mathbf{a}_c$, $\mathbf{b}_c$, or $\mathbf{c}_c$ axis. The second is a translational move by a distance chosen randomly in the interval $[-\delta_t, \delta_t]$ ($\delta_r = 0.3$ nm) along a randomly chosen direction of a random bead or nucleosome.

Both types of moves are accepted or rejected using the standard Metropolis criterion based on changes in the total energy of the system ΔE. That is, if $\Delta E < 0$, the move is accepted; and if $\Delta E > 0$, the move is accepted with a probability $\exp(-\Delta E/k_B T)$, where k_B is the Boltzmann constant and T is the temperature. In all cases, we allow the system to equilibrate for N_{eq} MC moves before the application of twist. We use 2×10^6 MC steps for each equilibration period.

The average twist in the exiting and entering linkers after equilibration is Tw^0_{ex} and Tw^0_{en}, respectively. After equilibration, the penultimate linker bead (bead 13 in Fig. 2, *left panel*) coordinate system is rotated about its local **a** axis by an angle $\Omega_0 = \pm\pi/4$. The system is then equilibrated again using the equilibration protocol. Rotations are applied unidirectionally, in either the clockwise or counterclockwise direction, which we denote by Ω_+ and Ω_-, respectively. Subsequent twist is applied using the same stepwise increments and equilibration phases. Fig. 2 shows a plot of the typical applied and induced twist-versus-MC steps. Our twisting method ensures sufficient time for relaxation between each subsequent twisting event, thus emulating the slow quasistatic twisting of chromatin in experiments.

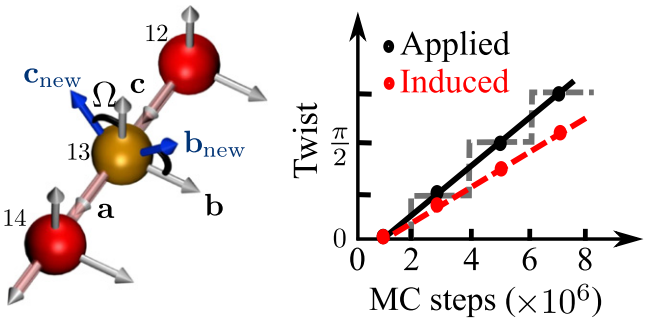

FIGURE 2 (*Left panel*) Twist is applied quasistatically by rotating the local coordinate system of the penultimate linker bead about its **a** axis by an angle Ω. (*Right panel*) Schematic of the applied and induced twist from the MC simulations.

We carry out a series of such twisting simulations at varying relative linker orientations, θ and ϕ, to probe their effects on the twisting response of the dinucleosome arrays. These angles are varied in increments of $\delta\theta = \pi/12$ and $\delta\phi = \pi/6$, in the range of $\theta \in (0, 2\pi)$, $\phi \in [-\pi/3, \pi/3]$.

RESULTS

Twist inversion

We define two parameters, k_{en} and k_{ex}, to characterize the fraction of imposed twist stored per linker segment in the exiting and entering linkers,

$$k_m = \frac{2\pi\left(Tw_m - Tw^0_m\right)}{N_m n \Omega_0}, \tag{7}$$

where $m = ex,en$, and where Tw_{ex} and Tw_{en} are the average twist in the exiting and entering linkers after n applications of twist, respectively. The twist in the two linkers is calculated as

$$Tw_{ex} = \frac{1}{2\pi}\left\langle \sum_{i=8}^{12}(\alpha_i + \gamma_i)\right\rangle, \tag{8}$$

$$Tw_{en} = \frac{1}{2\pi}\left\langle \sum_{i=1}^{7}(\alpha_i + \gamma_i)\right\rangle. \tag{9}$$

Note that the number of segments that absorb twist in the two linkers are different ($N_{ex} = 5$ and $N_{en} = 7$).

Fig. 3 shows k_{ex} and k_{en} versus θ for several ϕ for positive applied twist Ω_+ during the second phase of twist application $n = 2$. Both k_{ex} and k_{en} are ϕ-invariant to first-order, but depend strongly on θ. Here, $k_{ex} > 0$ for all θ- and ϕ-values while, interestingly, k_{en} is negative for a subset of θ. Regions where k_{ex} and k_{en} are opposite in sign imply inverted twist. $k_{en} = 0$ for a narrow range of θ corresponding to zero twist propagation.

Twist propagation can be more clearly characterized by defining $\Lambda = \mathrm{Sgn}(k_{en} \times k_{ex})$, where $\mathrm{Sgn}(x)$ is the sign of x and $\mathrm{Sgn}(0) = 0$, and $\Lambda > 0$, $\Lambda = 0$, and $\Lambda < 0$ correspond to conserved twist direction; zero twist propagation; and twist inversion, respectively. Fig. 4 shows twist in a dinucleosome with $\phi = -\pi/3$ subjected to negative applied twist. The upper panels of Fig. 4 (*left* to *right*) show representative plots of twist in the dinucleosome for $\theta = 3\pi/2$,

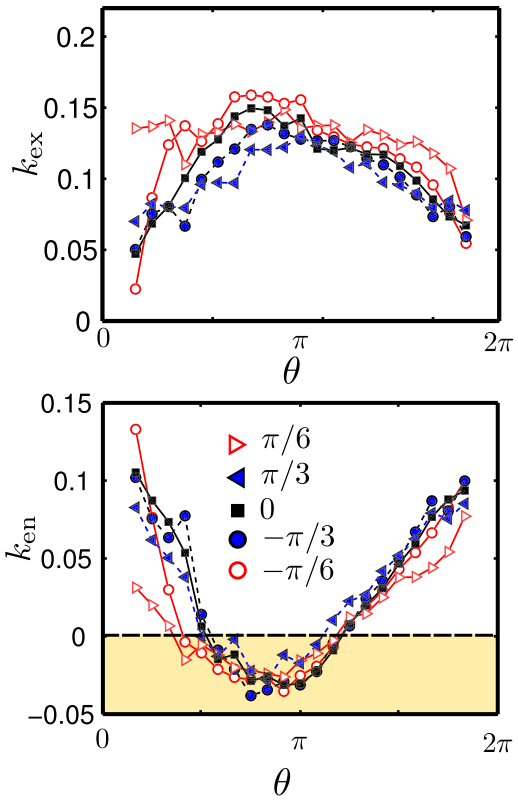

FIGURE 3 Plots of k_{ex} and k_{en} for various ϕ as a function of θ for positive applied twist, Ω_+, for a total applied twist of $\pi/2$. Twist inversion occurs when k_{ex} and k_{en} are opposite in sign.

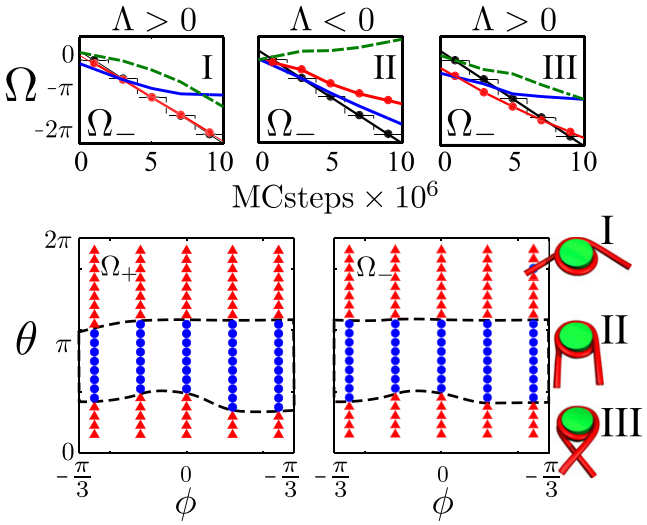

FIGURE 4 The top panel shows representative twist propagation results from our MC simulations for zones I ($\theta = 3\pi/2$), II ($\theta = \pi$), and III ($\theta = \pi/6$) for counterclockwise applied twist Ω_- and $\phi = -\pi/3$. Zone II is twist-inverting. (*Solid blue* and *dashed green lines*) Twist in the exiting and entering linker, respectively. (*Black* and *red lines*) Applied and induced total twist, respectively. (*Bottom panel*) Computed regimes of positive (*red triangles*) and negative (*blue triangles*) relative twists Λ for both directions of twist.

$\theta = \pi$, and $\theta = \pi/6$, respectively. Both cases for $\Lambda > 0$ show that the magnitude of twist in the exiting and entering linkers are increasing as the applied total twist increases. The center panel corresponding to $\Lambda < 0$ shows that the magnitude of twist in the exiting and entering linker are increasing, although in opposite directions. This corresponds to twist inversion in the dinucleosome.

We now construct phase diagrams which show relative linker twist-direction as functions of θ and ϕ. These phase diagrams are shown in the two lower panels of Fig. 4 for positive and negative applied twist. We define three twist propagation zones. Zones I and III ($\Lambda > 0$) are both twist-direction conserving. Zone II ($\Lambda < 0$), is twist-inverting. Fig. 4 also shows schematic linker conformations in each zone. Remarkably, the phase diagrams are invariant to ϕ and direction of applied twist. Phase boundaries shown by dashed lines illustrate zero twist propagation, $\Lambda = 0$.

We provide a simple explanation of twist inversion that accounts for relative linker orientation and nucleosome geometry. Our Ansatz is that nucleosomes rotate as rigid bodies, resulting from the strong DNA/nucleosome binding. Applied rotations on the exiting linker induce nucleosome rotations, which, in turn, induce rotations in the entering linker. We define $\mathbf{\Gamma}_i = \{\mathbf{a}_i, \mathbf{b}_i, \mathbf{c}_i\}$ and $\mathbf{\Gamma}'_i = \{\mathbf{a}'_i, \mathbf{b}'_i, \mathbf{c}'_i\}$ to be the coordinate systems before and after rotation of the exiting linker, respectively. As shown in Fig. 5, $\mathbf{\Gamma}_0$ is the coordinate system of the entering linker bead, which we assume to be fixed for our argument; $\mathbf{\Gamma}_1$ is the coordinate system of the entering linker attachment point; $\mathbf{\Gamma}_2$ is the coordinate system of the exiting linker attachment point; and $\mathbf{\Gamma}_3$ is the coordinate system of exiting bead being rotated anticlockwise. That is, the axes $\mathbf{b}'_3$ and $\mathbf{c}'_3$ are rotated while $\mathbf{a}_3$ remains unchanged. A rotation is induced in $\mathbf{\Gamma}_2$ about the $\mathbf{a}_2$ axis, thus rotating the nucleosome. The induced rotation about $\mathbf{a}_2$ is always smaller in magnitude than the applied rotation, resulting from the linker's finite torsional rigidity.

Fig. 5, *a–c*, shows the effect of applied rotation of $\mathbf{\Gamma}_3$ for three entry/exit angles: $\theta = 180°$, $360°$, and $270°$, respectively. For $\theta = 180°$, the nucleosome rotation causes rotation of $\mathbf{\Gamma}_1$ about the $\mathbf{a}_1$ axis. The relative coordinate system rotations and directions required to go from $\mathbf{\Gamma}_0 \rightarrow \mathbf{\Gamma}_1'$ and $\mathbf{\Gamma}_2' \rightarrow \mathbf{\Gamma}_3'$ are also shown. In fact, the above two rotations are by definition described by the angles $(\alpha_0 + \gamma_0)$ and $(\alpha_2 + \gamma_2)$, the twists in the entering and exiting linkers, respectively. Clearly, the two linker twists are opposite in sign, thus resulting in twist inversion across the central nucleosome. Similar arguments apply for $\theta = 360°$ (and $0°$) as demonstrated in Fig. 5 *b*. Here, the direction of rotations $(\alpha_0 + \gamma_0)$ and $(\alpha_2 + \gamma_2)$ required to transform $\mathbf{\Gamma}_0 \rightarrow \mathbf{\Gamma}_1'$ and $\mathbf{\Gamma}_2' \rightarrow \mathbf{\Gamma}_3'$, respectively, have the same sign. Thus, the twists in the two linkers are of the same sign. Finally, Fig. 5 *c* shows the $\theta = 270°$ (and $90°$) case. By definition, the Euler angles α_0 and γ_0 can be calculated from the relationship (27)

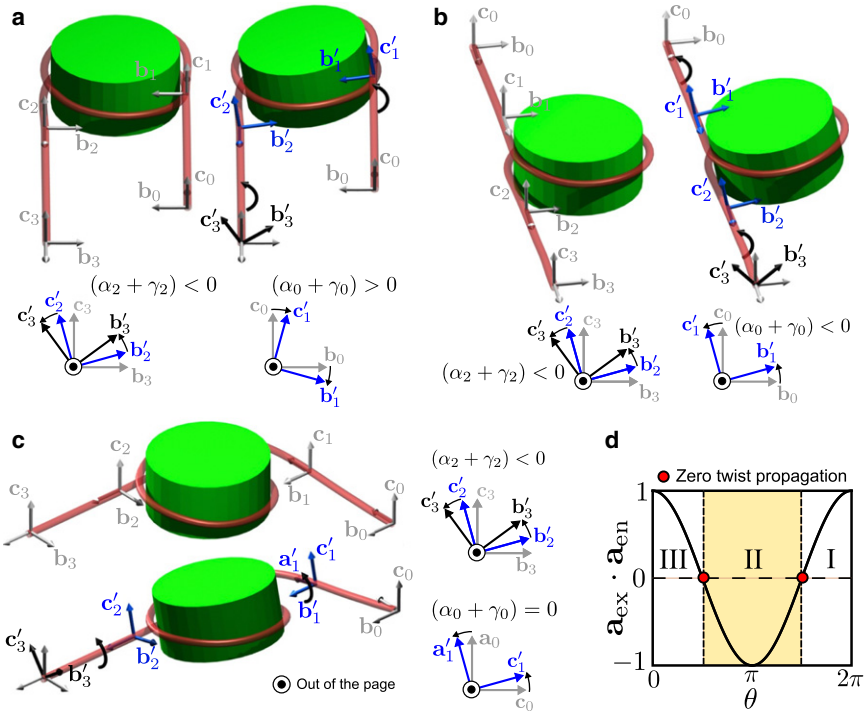

FIGURE 5 Effect of applied twist on the linker and nucleosome coordinate systems for three different values of θ: (*a*) twist sign inversion $\theta = \pi$, (*b*) twist sign conservation $\theta = 2\pi$, and (*c*) zero twist propagation example for $\theta = \pi/2$. (*d*) Twist inversion zones obtained from a calculation of the dot product of $\mathbf{a}_{ex} \cdot \mathbf{a}_{en} = \cos(\theta)$. Values of $\mathbf{a}_{ex}$,$\mathbf{a}_{en} = \cos(\theta) < 0$ imply twist inversion.

$$\cos(\alpha_0 + \gamma_0) = \frac{\mathbf{b}_0\cdot\mathbf{b}_1' + \mathbf{c}_0\cdot\mathbf{c}_1'}{1 + \mathbf{a}_0\cdot\mathbf{a}_1'}. \tag{10}$$

By examining the relative rotations of the coordinate systems, it can be deduced that $(\alpha_0 + \gamma_0) = 0$, as $\mathbf{a}_0\cdot\mathbf{a}_1' = \mathbf{c}_0\cdot\mathbf{c}_1'$ and $\mathbf{b}_0\cdot\mathbf{b}_1' = 1$. Consequently, $\theta = 90°$ (and 270°) yields zero twist propagation.

To generalize the argument, we consider $\mathbf{\Gamma}_{ex}$ and $\mathbf{\Gamma}_{en}$ to be the exiting and entering linker attachment coordinate systems for a nucleosome lying flat across the $\hat{\mathbf{x}} - \hat{\mathbf{y}}$ plane. We fix the exiting coordinate system $\mathbf{a}_{ex} = \hat{\mathbf{x}}$. For the angle θ (and $\phi = 0$), $\mathbf{a}_{en}$ is then given by $\cos(\theta)\hat{\mathbf{x}} + \sin(\theta)\hat{\mathbf{y}}$ in terms of the unit vectors $\hat{\mathbf{x}}$ and $\hat{\mathbf{y}}$. Varying θ alters the relative orientations of $\mathbf{a}_{ex}$ and $\mathbf{a}_{en}$. The sign of the dot product, $\mathbf{a}_{ex} \cdot \mathbf{a}_{en} = \cos(\theta)$, gives the relative twist direction in the linkers. A plot of $\mathbf{a}_{ex} \cdot \mathbf{a}_{en}$ vs. θ is shown in Fig. 5 *d*: $\cos(\theta) = 0$ for $\theta = \pi/2, 3\pi/2$ yields zero twist propagation; $\mathbf{a}_{ex} \cdot \mathbf{a}_{en} < 0$ for $\theta \in (\pi/2, 3\pi/2)$ corresponds to twist inversion; and the twist direction is conserved otherwise.

Our geometric argument illustrates the physical origin of twist inversion in the dinucleosome. It also provides a good first-order approximation of the dependence of the angle θ on twist inversion. Twist propagation in the dinucleosome is actually more complex. For instance, our explanation does not account for: linker twist/bend coupling, internucleosome interactions, steric effects, and effects arising from the size of the nucleosome. We also do not predict the magnitude of the twist propagated, only its sign. These additional effects may account for the observed differences in our predicted twist inversion zones and boundaries and those obtained by simulation.

Nucleosome flipping

Continued twisting of the dinucleosome leads to the second interesting finding of this study: the unconstrained nucleosome may undergo a sudden reorientation that we refer to as "nucleosome flipping". This effect is best illustrated by examining the continued twisting of a representative dinucleosome with $\theta = 225°$ and $\phi = 0°$ for counterclockwise-applied twist. Fig. 6 *a* shows a series of snapshots of the dinucleosome conformation versus MC steps. Initially, the unconstrained nucleosome's orientation remains unchanged. At ~1.5 $\times$ 10^7 MC steps, it rapidly inverts, and the linker bends sharply. Similar flipping events were observed in several other simulations. The finite twist storage capability of linkers and fast flipping of the nucleosomes is analogous to observed jump or buckling instabilities in end-clamped finite semirigid rods that are twisted at one end (29,30). At a critical applied twist, the rods buckle and form loops, thus converting their twist into writhe over very short times, which is qualitatively similar to observed buckling in our dinucleosome.

Three key features are associated with nucleosome flipping events:

First, nucleosome flipping correlates with an exchange of the twist in the two linkers. Fig. 6 *b* shows the average twist in the linker beads adjacent to the free-nucleosome-versus-MC steps. The magnitude of twist in the exiting linker bead

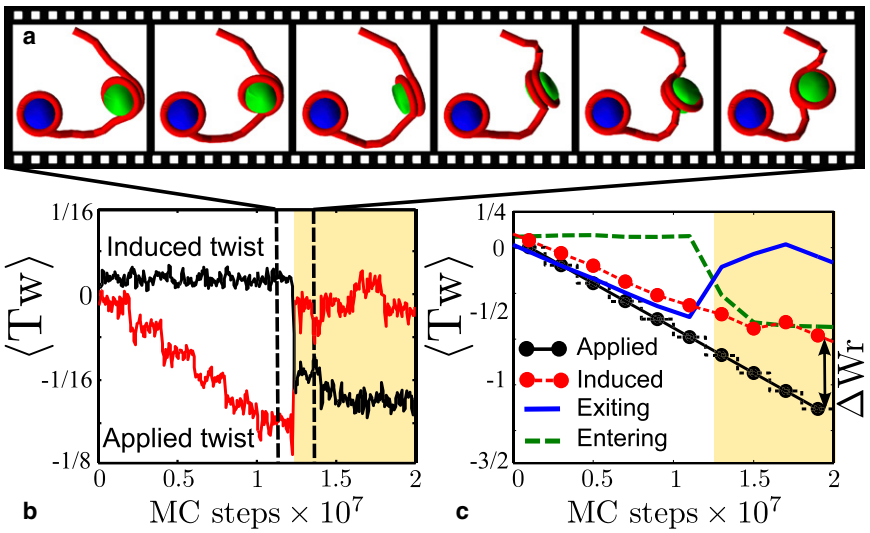

FIGURE 6 Nucleosome flipping dynamics for dinucleosomes with $\theta = 225^\circ$ and $\phi = 0^\circ$. (*a*) Series of snapshots from the MC simulations showing evolution of the dinucleosome conformations and associated nucleosome flipping and linker buckling. (*b*) Applied and induced twist in linkers on the exiting (*red*) and entering linkers (*black*), respectively. (*c*) Total applied and induced twist (*solid black* and *red lines*) and the total twist on exiting and entering linker beads adjacent to the nucleosome (*dashed green* and *solid blue lines*).

increases with larger applied twist. At ~1.5×10^7 MC steps, twist propagates from the exiting to the entering linkers. This results in a steep change in the exiting and entering linker twists, respectively. Clearly, this exchange is the largest for cases where the two twists are of opposite sign with respect to each other. Indeed, we observe nucleosome flipping to be most abrupt for intermediate θ-values, corresponding to the observed range of twist inversion, and more gradual for small and large θ-values.

Second, an exchange of energy between the different modes accompanies nucleosome flipping. Fig. 7 shows the evolution of stretching (E_{str}), twisting (E_{Tw}), bending (E_{bend}), and Coulombic-plus-excluded-volume (E_{EVC}) energy contributions versus MC steps for the above system. Before flipping ($<10^7$ MC steps), E_{Tw} increases in the same steplike manner as the applied twist. The step height increases quadratically, as a result of E_{Tw}'s quadratic dependence on applied twist. We also observe slight increases in E_{bend}, E_{str}, and E_{EVC}, likely due to the coupling between the bending and twisting modes, the stretching of bent linkers, and increased electrostatic repulsion between the nucleosomes, respectively. At the onset of flipping, E_{bend} rapidly increases while E_{Tw} stabilizes. Here, the twisting energy penalty begins to exceed that associated with the sharp bending of the linkers, thus relieving some of the linker torsional stress. At this point, linker buckling also induces the abrupt nucleosome flipping, followed by additional equilibration of the bending and twisting energies. Upon flipping, E_{EVC} also decreases, possibly as a result of increased separation of the linkers and thereby reduced electrostatic repulsion. We further note that flipping occurs at ~$E_{Tw} = 22$ kcal/mol (~37 k_BT). Other simulations with different θ and ϕ, in which nucleosome flipping occur, yield similar energy barriers, perhaps suggesting a universality in the energy required for nucleosome flipping. Note that the above value is a very rough estimate of the free energy barrier, as it excludes various contributions including conformational entropy. It would be interesting to examine the energetics and kinetics of nucleosome flipping in more detail.

Third, the imposed twist is not equal to the net observed twist, which can be interpreted as a change in the overall writhe of the system. Fig. 6 *c* shows the average applied and induced twist in the system along with the total twist in both linkers. The difference between the induced and applied twist can be explained in terms of the linking number, *Lk*, given by the sum of the twist and writhe, $Lk = Tw + Wr$. Although, strictly speaking, this relationship is only applicable to closed curves, we apply it to the

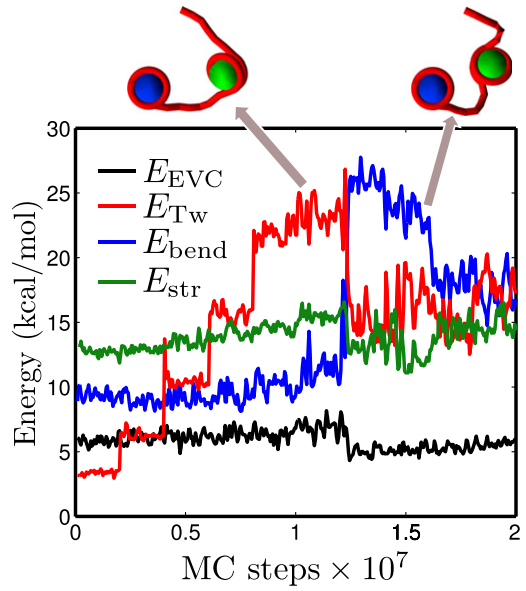

FIGURE 7 Dinucleosome energy contributions from twist E_{Tw}, bending E_{bend}, stretching E_{str}, and excluded volume plus Coulombic interactions E_{EVC} for dinucleosome simulations with $\theta = 225^\circ$ and $\phi = 0^\circ$.

dinucleosome under the assumption that the constrained ends are connected by a phantom curve. Similar approaches have been used by others to estimate writhe in open curves (15,31,32). The change in linking number ΔLk is then equal to $\Delta Tw + \Delta Wr - Tw_{ap}$, where Tw_{ap} is the applied twist. Because $\Delta Lk = 0$ for closed curves, $\Delta Wr = Tw_{ap} - \Delta Tw$ and a numerical estimate of twist-to-writhe conversion is the difference in the applied and induced twist.

To better illustrate this point, we present an additional system with $\theta = 90^\circ$ and $\phi = 60^\circ$ that undergoes a larger conformation change (Fig. 8). As with the previous example, applied and induced twist are not equal. The spontaneous occurring twist during the equilibration of the array is denoted $Tw^0 (= Tw^0_{ex} + Tw^0_{en})$. At the end of the simulation $\Delta Wr \simeq -0.64$, illustrating the significant change in the overall writhe. The change in writhe is correlated with a conformational change of the dinucleosome. Fig. 8 also shows the initial and final conformation of the dinucleosome. The dashed red line indicates that the dinucleosome is treated as a closed loop. We approximate the directional writhe as the sum of the signed crossings of the projection of the linker path onto a plane. The writhes for the initial and final conformations are $Wr = 0$ and $Wr = -1$, yielding $\Delta Wr = -1$. Thus, the directional writhe change computed from the above approximate approach exhibits the same sign as that computed from the difference in the measured and applied twists—further confirming twist-to-writhe conversion in nucleosome flipping.

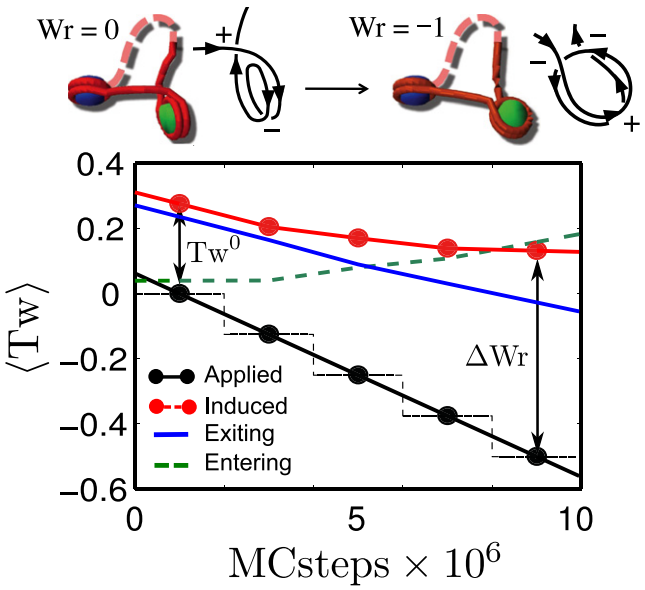

FIGURE 8 Total applied and induced twist (*solid black* and *red lines*) and the total twist on exiting and entering linker beads adjacent to the nucleosome (*dashed green* and *solid blue lines*) for $\theta = 90^\circ$ and $\phi = 60^\circ$. Tw^0 is the spontaneously occurring twist in the linker after equilibration and ΔWr is the change in writhe of the system at the end of the simulation. Also shown are the starting and final dinucleosome conformations and the projections of their linker paths onto a plane for counting the number of positive and negative crossings for directional writhe calculations. (*Dashed red line*) Phantom curve drawn to close the linker trajectory.

DISCUSSION

Our simulations furnish two intriguing observations about twist propagation in dinucleosome arrays:

First, applied twist may lead to inverted twist in contiguous linkers. This phenomenon is a result of strong DNA/octamer binding that inhibits twist propagation along the wound DNA; twist propagation instead occurs via rigid-body-like rotations of the entire nucleosome. Hence, twist inversion is strongly dependent on the relative orientation of contiguous linkers at their point of entry and exit to the nucleosome.

Second, continued twisting in dinucleosome arrays may lead to nucleosome flipping and associated linker buckling. The latter occurs to relieve excessive stored twist in one linker; nucleosome flipping events facilitate quick transfer between contiguous linkers and also results in conversion of twist to writhe.

Our twist inversion finding leads to the obvious question: Can twist inversion occur in real chromatin fiber?

Our simulations suggest that a single parameter, the entry/exit angle θ, dictates twist inversion, and that angles in the range $90^\circ \lessapprox \theta \lessapprox 220^\circ$ are required for twist inversion to occur. The entry/exit angles in the nucleosome crystal structure, θ_0, are in the range 108°–126° (22), corresponding to 1.65–1.7 turns of wound DNA, well within the predicted range of twist inversion. However, θ is dependent on salt conditions, and even at fixed salt conditions, θ exhibits large variations due to spontaneous unwrapping of DNA (33). At low salt concentrations, chromatin exhibits an unfolded conformation. The strong repulsion between the entering and exiting linkers causes them to diverge, resulting in a large increase in θ, potentially exceeding the upper angle limit of twist inversion. In contrast, at high salt conditions, chromatin is tightly folded and the wound DNA likely maintains its original entry/exit angle θ_0. Hence, we expect unfolded chromatin at low salt concentrations to exhibit unidirectional twist and strongly folded chromatin at physiological salt conditions to exhibit twist inversion (bimodal twist). Because the nucleosomes exhibit more restricted dynamics in chromatin fibers due to packing and histone tail interactions, it is difficult to extrapolate how far the unidirectional and inverted twists propagate along the fiber from our single-nucleosome results.

What are the possible implications of twist inversion?

One possibility is that twist inversion could allow creation of alternate regions of overwound and underwound DNA, which could potentially have specific roles in chromatin function. Some proteins are known to preferentially bind to either over- or underwound DNA (9,34–36). For example, the activity of the 434 repressor is dictated by the degree to which DNA is wound at its operator site (36). Also,

architectural proteins such as SRY prefer binding to overtwisted DNA while zinc finger proteins prefer undertwisted DNA (35). Opposite twists on contiguous linkers could therefore potentially enhance interactions between over- and underwound DNA-binding proteins. Twist inversion could also play a role in chromatin dynamics, especially under external twisting, as the direction of nucleosome rotation depends on the twists in the entering and exiting linkers. In addition, coupling between twist-inverting and non-twist-inverting zones could modulate local nucleosome rotations, providing a method to modify local chromatin conformation and to locally over- or under-twist chromatin, depending on its topology.

The continued twisting of dinucleosomes induces sharp bending of the linker. Because some DNA sequences are more susceptible to bending than others, such torsion-driven buckling may provide a mechanism to modulate site-specific bending in chromatin (37). Localized buckling could synergize the binding of specific regulatory proteins that preferentially bind to curved DNA. In particular, TATA sequences that play a key role in transcription by binding to various transcriptional factors are prone to bending. Hence, torsional forces from various cellular machinery could potentially instigate conformational changes near stress-sensitive sites, such as TATA boxes, to regulate the transcriptional activity of chromatin (38). If these torques induce nucleosome flipping and buckling of linker, it may provide a method of governing local protein binding that could regulate protein binding and transcription. The conversion of twist to bending via local buckling of DNA may also serve as a transient reservoir or dynamic buffer to absorb twist in chromatin without causing drastic changes in its conformation (38). The dependence of the abruptness of nucleosome flipping on linker orientation may also play an as-yet-unknown role in chromatin's ability to transiently absorb torsional stress.

Our energetic analysis indicates that significant twist can be applied before inducing nucleosome flipping. If, for example, the applied twist originates from an advancing polymerase that exerts torques of ~1.25 k_BT/rad, flipping would occur after ± 6 polymerase rotations, corresponding to the ~37 k_BT energy barrier observed in our simulations. In our example, the ~180° nucleosome flipping transition occurs after ~270° of twist has been applied. The high energetic barrier of flipping indicates that dinucleosomes can transiently absorb applied twist and act as reservoirs for applied twist. Chromatin's strong twist storing capacity contrasts sharply with that of DNA, testifying to chromatin's structural stability. Larger chromatin arrays will undoubtedly exhibit a more complex interplay among twist, bending, and internucleosome interactions, and much remains to be understood about their fundamental physics, including how they propagate twist.

In summary, we expect that twist inversion and nucleosome flipping are real phenomena that could play important roles in chromatin function. It may be possible to verify their existence experimentally using, for instance, single molecule techniques (24).

CONCLUSIONS

We have presented a systematic Monte Carlo study of the torsional response of end-constrained dinucleosome arrays. Our results suggest that the propagation of twist within a dinucleosome strongly depends on the relative orientation of contiguous DNA linkers, a subset of which leads to inverted twist. Our intuitive explanation of twist inversion illustrates how simple constraints on DNA imposed by the nucleosome lead to very unexpected consequences for twist propagation along DNA in nucleosome arrays. Our results also demonstrate how dinucleosomes subjected to continued twisting can undergo dramatic conformational changes, nucleosome flipping. This flipping occurs at energy barriers that indicate chromatin's significant ability to transiently store twist. Our study thus demonstrates how simple modeling and simulations provide an effective tool to probe nucleosome dynamics and to uncover previously unknown properties of chromatin. Continued modeling efforts, at varying levels of complexity, will undoubtedly uncover more fundamental details of chromatin dynamics. Specifically, our future work will focus on the torsional properties of large chromatin arrays containing tens to hundreds of nucleosomes, with the aim of detailing how applied torsion affects chromatin higher-order structure.

SUPPORTING MATERIAL

One table and two figures are available at http://www.biophysj.org/biophysj/supplemental/S0006-3495(10)01205-1.

Computer time on the Granite cluster of the Bioengineering department at the University of California at San Diego is acknowledged. The authors acknowledge various discussions with Dario Meluzzi, Balaji Iyer, Darren Yang, and Arijit Maitra.

G.A. thanks the Hellman Fellowship and the Chancellor's Interdisciplinary Collaboratories program at the University of California at San Diego for funding.

REFERENCES

1. Alberts, B., A. Johnson, …, P. Walter. 2002. Molecular Biology of the Cell. Garland Science, New York.
2. Lavelle, C. 2008. DNA torsional stress propagates through chromatin fiber and participates in transcriptional regulation. *Nat. Struct. Mol. Biol.* 15:123–125.
3. Bancaud, A., G. Wagner, …, A. Prunell. 2007. Nucleosome chiral transition under positive torsional stress in single chromatin fibers. *Mol. Cell.* 27:135–147.
4. Liu, L. F., and J. C. Wang. 1987. Supercoiling of the DNA template during transcription. *Proc. Natl. Acad. Sci. USA.* 84:7024–7027.
5. Strick, T. R., J. F. Allemand, …, V. Croquette. 1998. Behavior of supercoiled DNA. *Biophys. J.* 74:2016–2028.

6. Ng, H.-L., and R. E. Dickerson. 2002. Mediation of the A/B-DNA helix transition by G-tracts in the crystal structure of duplex CATGGGCC-CATG. *Nucleic Acids Res.* 30:4061–4067.
7. Charvin, G., J.-F. Allemand, …, V. Croquette. 2004. Twisting DNA: single molecule studies. *Contemp. Phys.* 45:383–403.
8. Imbalzano, A. N., H. Kwon, …, R. E. Kingston. 1994. Facilitated binding of TATA-binding protein to nucleosomal DNA. *Nature.* 370:481–485.
9. Hatfield, G. W., and C. J. Benham. 2002. DNA topology-mediated control of global gene expression in Escherichia coli. *Annu. Rev. Genet.* 36:175–203.
10. Lynch, T. W., E. K. Read, …, P. A. Rice. 2003. Integration host factor: putting a twist on protein-DNA recognition. *J. Mol. Biol.* 330:493–502.
11. Mazur, A. K. 2010. Anharmonic torsional stiffness of DNA revealed under small external torques. *Phys. Rev. Lett.* 105:018102.
12. Schoeffler, A. J., and J. M. Berger. 2008. DNA topoisomerases: harnessing and constraining energy to govern chromosome topology. *Q. Rev. Biophys.* 41:41–101.
13. Nitiss, J. L. 2009. DNA topoisomerase II and its growing repertoire of biological functions. *Nat. Rev. Cancer.* 9:327–337.
14. Kouzine, F., S. Sanford, …, D. Levens. 2008. The functional response of upstream DNA to dynamic supercoiling in vivo. *Nat. Struct. Mol. Biol.* 15:146–154.
15. Rossetto, V., and A. C. Maggs. 2003. Writhing geometry of open DNA. *J. Chem. Phys.* 21:9864–9874.
16. Meluzzi, D., D. E. Smith, and G. Arya. 2010. Biophysics of knotting. *Annu. Rev. Biophys.* 39:349–366.
17. Smith, S. B., Y. Cui, and C. Bustamante. 1996. Overstretching B-DNA: the elastic response of individual double-stranded and single-stranded DNA molecules. *Science.* 271:795–799.
18. Strick, T. R., J.-F. Allemand, …, V. Croquette. 1996. The elasticity of a single supercoiled DNA molecule. *Science.* 271:1835–1837.
19. Wereszczynski, J., and I. Andricioaei. 2006. On structural transitions, thermodynamic equilibrium, and the phase diagram of DNA and RNA duplexes under torque and tension. *Proc. Natl. Acad. Sci. USA.* 103:16200–16205.
20. Klenin, K., and J. Langowski. 2000. Computation of writhe in modeling of supercoiled DNA. *Biopolymers.* 54:307–317.
21. Merlitz, H., K. Rippe, …, J. Langowski. 1998. Looping dynamics of linear DNA molecules and the effect of DNA curvature: a study by Brownian dynamics simulation. *Biophys. J.* 74:773–779.
22. Davey, C. A., D. F. Sargent, …, T. J. Richmond. 2002. Solvent mediated interactions in the structure of the nucleosome core particle at 1.9 Å resolution. *J. Mol. Biol.* 319:1097–1113.
23. Felsenfeld, G., and M. Groudine. 2003. Controlling the double helix. *Nature.* 421:448–453.
24. Bancaud, A., N. Conde e Silva, …, J. L. Viovy. 2006. Structural plasticity of single chromatin fibers revealed by torsional manipulation. *Nat. Struct. Mol. Biol.* 13:444–450.
25. Gupta, P., J. Zlatanova, and M. Tomschik. 2009. Nucleosome assembly depends on the torsion in the DNA molecule: a magnetic tweezers study. *Biophys. J.* 97:3150–3157.
26. Celedon, A., I. M. Nodelman, …, S. X. Sun. 2009. Magnetic tweezers measurement of single molecule torque. *Nano Lett.* 9:1720–1725.
27. Arya, G., Q. Zhang, and T. Schlick. 2006. Flexible histone tails in a new mesoscopic oligonucleosome model. *Biophys. J.* 91:133–150.
28. Beard, D. A., and T. Schlick. 2001. Computational modeling predicts the structure and dynamics of chromatin fiber. *Structure.* 9:105–114.
29. Neukirch, S., G. H. M. van der Heijden, and J. M. T. Thompson. 2002. Writhing instabilities of twisted rods: from infinite to finite length. *J. Mech. Phys. Solids.* 50:1175–1191.
30. van der Heijden, G. H. M., S. Neukirch, …, J. M. T. Thompson. 2003. Instability and self-contact phenomena in the writhing of clamped rods. *Int. J. Mech. Sci.* 45:161–196.
31. van der Heijden, G. H. M., M. A. Peletier, and R. Planque. 2007. On-end rotation for open rods undergoing large deformations. *Q. Appl. Math.* 65:385–402.
32. Starostin, E. L. 2005. On the writhe of non-closed curves. Physical and Numerical Models in Knot Theory. World Scientific, Singapore, pp. 525–545.
33. Polach, K. J., and J. Widom. 1995. Mechanism of protein access to specific DNA sequences in chromatin: a dynamic equilibrium model for gene regulation. *J. Mol. Biol.* 254:130–149.
34. Remus, D., E. L. Beall, and M. R. Botchan. 2004. DNA topology, not DNA sequence, is a critical determinant for *Drosophila* ORC-DNA binding. *EMBO J.* 23:897–907.
35. Rohs, R., X. Jin, …, R. S. Mann. 2010. Origins of specificity in protein-DNA recognition. *Annu. Rev. Biochem.* 79:233–269.
36. Koudelka, G. B. 1998. Recognition of DNA structure by 434 repressor. *Nucleic Acids Res.* 26:669–675.
37. Kouzine, F., J. Liu, …, D. Levens. 2004. The dynamic response of upstream DNA to transcription-generated torsional stress. *Nat. Struct. Mol. Biol.* 11:1092–1100.
38. Lavelle, C., J.-M. Victor, and J. Zlatanova. 2010. Chromatin fiber dynamics under tension and torsion. *Int. J. Mol. Sci.* 11:1557–1579.